Small-scale variation of snow in a regional permafrost model

K. Gisnås[1], S. Westermann[1], T.V. Schuler[1], K. Melvold[2] and B. Etzelmüller[1]

[1] Department of Geosciences, University of Oslo, Oslo, Norway

[2] Norwegian Water Resources and Energy Directorate, Oslo, Norway

Corresponding author: Kjersti Gisnås (kjersti.gisnas@geo.uio.no)

Abstract

The strong winds prevalent in high altitude and arctic environments heavily redistribute the snow cover, causing a small-scale pattern of highly variable snow depths. This has profound implications for the ground thermal regime, resulting in highly variable near-surface ground temperatures on the meter scale. Due to asymmetric snow distributions combined with the non-linear insulating effect of snow, the spatial average ground temperature in a 1km² area cannot be determined based on the average snow cover for that area. Land surface or permafrost models employing a coarsely classified average snow depth will therefore not yield a realistic representation of ground temperatures. In this study we employ statistically derived snow distributions within 1km² grid cells as input to a regional permafrost model in order to represent sub-grid variability of ground temperatures. This improves the representation of both the average and the total range of ground temperatures. The model reproduce observed sub-grid ground temperature variations of up to 6°C, and 98% of borehole observations match the modelled temperature range. The mean modelled temperature of the grid cell reproduces the observations with an accuracy of 1.5°C or better. The observed sub-grid variations in ground surface temperatures from two field sites are very well reproduced, with estimated fractions of sub-zero *MAGST* within ±10%. We also find that snow distributions within areas of 1km² in Norwegian mountain environments are closer to a *gamma* than to a *lognormal* theoretical distribution. The modelled permafrost distribution seems to be more sensitive to the choice of distribution function than to the fine-tuning of the

1 coefficient of variation of the distribution. When incorporating the small-scale variation of

2 snow, the modelled total permafrost area of mainland Norway is nearly twice as large

3 compared to the area obtained with grid-cell average snow depths without a sub-grid

4 approach.

5

6 **1   Introduction**

7 High altitude and arctic environments are exposed to strong winds and drifting snow can

8 create a small-scale pattern of highly variable snow depths. Seasonal snow cover is a crucial

9 factor for the ground thermal regime in these areas (e.g. Goodrich, 1982; Zhang et al., 2001).

10 This small-scale pattern of varying snow depths results in highly variable ground surface

11 temperatures on the meter scale of up to 6 °C in areas of less than 1 km^2 (e.g. Gubler et al.,

12 2011; Gisnås et al., 2014). Grid-based numerical land surface and permafrost models operate

13 on scales too coarse to resolve the variability of snow depths, and are not capable of

14 representing such small-scale variability. For the Norwegian mainland, permafrost models

15 have been implemented with a spatial grid resolution of 1 km^2 (Gisnås et al., 2013;

16 Westermann et al., 2013), and do therefore only represent the larger scale patterns of ground

17 temperatures. As a consequence, they usually represent the lower limit of permafrost as a

18 sharp boundary, where the average ground temperature of a grid-cell crosses the freezing

19 temperature (0°C). In reality, the lower permafrost boundary is a fuzzy transition. Local

20 parameters, such as snow cover, solar radiation, vegetation, soil moisture and soil type cause a

21 pronounced sub-grid variation of ground temperature. Different approaches have been

22 developed to address this mismatch of scales, such as the TopoSub (Fiddes and Gruber,

23 2012), accounting for the variability of a range of surface parameters using k-means

24 clustering. At high latitudes and altitudes, one of the principal controls on the variability of

25 ground temperature is the effect of sub-grid variation in snow cover (e.g. Langer et al., 2013).

26 The observed variability in ground surface temperatures within 1 km x 1 km areas is to a large

27 degree reproduced by only accounting for the variation in snow depths (Gisnås et al., 2014).

28 Therefore, procedures capable of resolving the small scale variability of snow depths could

29 considerably improve the representation of the ground thermal regime.

30 The spatial variation of snow is a result of several mechanisms operating on different scales in

31 different environments (Liston et al. 2004). In tundra and alpine areas, wind-affected

32 deposition is the dominant control on the snow distribution at distances below 1 km (Clark et

al., 2011). Physically-based snow distribution models are useful over smaller areas, but are not applicable on a regional scale. The coefficient of variation (CV), defined as the ratio between the standard deviation and the mean, is a measure of the extent of spread in a distribution. The coefficient of variation of snow depths (CV_{sd}) typically range from low spread at 0.2 to high spread at 0.8, which suits snow distributions in a range of environments (e.g. Liston, 2004; Winstral and Marks, 2014). Liston (2004) assigned individual values of CV_{sd} to different land use classes in order to address sub-grid variability of snow in land surface schemes. According to this scheme, non-forested areas in Norway, as well as most of the permafrost areas in northern Europe ("*high-latitude alpine areas*"), would have been allocated a CV_{sd} of *0.7*. A review of observed CV_{sd} from a large number of snow surveys in the northern hemisphere shows a large spread of CV_{sd} values, in particular within this land use class, ranging from *0.1* to *0.9* (Clark et al., 2011). This illustrates the need for improved representation of snow distribution within this land use class.

An accurate representation of the small scale snow variation influences the timing and magnitude of runoff in hydrological models, and a detailed picture of the sub-grid variability is of great value for the hydropower industry and flood forecasting. Adequate representations of the snow covered fraction in land surface schemes improve simulated near surface air temperatures, ground temperatures and evaporation due to the considerable influence of snow cover on the duration of melt season and the surface albedo.

In this study we derive functional dependencies between distributions of snow depth within 1x1 km grid cells and CV_{sd}, based on an extensive in-situ data set from Norwegian alpine areas. In a second step, we employ the resulting snow distributions as input to the permafrost model CryoGRID1, a spatially distributed, equilibrium permafrost model (Gisnås et al., 2013). Using a sub-grid representation of ground temperatures, permafrost probabilities are derived, hence enabling a more realistic, fuzzy permafrost boundary instead of a binary, sharp transition. With this approach, we aim to improve permafrost distribution modelling in inhomogeneous terrains.

2   Setting

The model is implemented for the Norwegian mainland, extending from 58° to 71°N. Both the topography and climate in Norway is dominated by the Scandes, a mountain range stretching south-north through Norway, separating the coastal western part with steep

mountains and deep fjords from the eastern part where the mountains gradually decrease in height. The maritime climate of the west coast is dominated by low-pressure systems from the Atlantic Ocean resulting in heavy precipitation, while the eastern parts of the Scandes have a more continental and drier climate. Mountain permafrost is present all the way to the southern parts of the Scandes, with a gradient in the lower limit of permafrost from c. 1400 to 1700 m from east to west in central southern Norway, and from c. 700 to 1200 m from east to west in northern Norway (Gisnås et al., 2013). While permafrost is also found in mires at lower elevations both in southern and northern Norway, most of the permafrost is located in exposed terrain above the tree line where strong winds result in heavy redistribution of snow.

The in-situ records of snow depth data used to establish the snow distribution scheme were collected at the Hardangervidda mountain plateau in the southern part of the Scandes (Fig. 1). It is the largest mountain plateau in northern Europe, located at elevations from 1000 to above 1700 meters a.s.l., with occurrences of permafrost in the highest mountain peaks. The terrain is open and slightly undulating in the east, while in the west it is more complex with steep mountains divided by valleys and fjords. The mountain range represents a significant orographic barrier for the prevailing westerly winds from the Atlantic Ocean, giving rise to large variations in precipitation and strong winds, two agents promoting a considerably wind-affected snow distribution. Mean annual precipitation varies from 500 to more than 3000 mm over distances of a few tens of kilometres, and maximum snow depths can vary from 0 to more than 10 meters over short distances (Melvold and Skaugen, 2013).

3   Model description

3.1   A statistical model for snow depth variation

The Winstral terrain-based approach (Winstral et al., 2002) is applied over the entire Norwegian mainland using the 10-meter national digital terrain model from the Norwegian Mapping Authority (available at Statkart.no), with wind data from the NORA10 dataset (Section 4.1) used to indicate the distribution of prevailing wind directions during the accumulation season.

The terrain-based exposure parameter (Sx), described in detail in (Winstral et al., 2002), quantifies the extent of shelter or exposure of the considered grid-cell. Sx is determined by the slope between the grid-cell and the cells of greatest upward slope in the upwind terrain. The

1   upwind terrain is defined as a sector towards the prevailing wind direction *d* constrained by

2   the maximum search distance (*dmax* = 100 m) and a chosen width (*A*) of 30° with the two

3   azimuths extending 15° to each side of *d* (see Fig. 2). The cell of the maximum upward slope

4   is identified for each search vector, separated by 5° increments. This gives in total seven

5   search vectors for each of the eight 30° wide sectors. *Sx* for the given grid-cell is finally

6   calculated as the average of the maximum upward slope gradient of all seven search vectors:

7   $$Sx_{d,A,dmax}(x_i y_i) = max \left[\tan\left(\frac{Z(x_v,y_v) - Z(x_i,y_i)}{[(x_v - x_i)^2 + (y_v - y_i)^2]^{0.5}}\right) \right] \qquad (1)$$

8   where *d* is the prevailing wind direction, *(x_i, y_i)* are the coordinates of the considered grid-cell,

9   and *(x_v, y_v)* are the sets of all cell coordinates located along the search vector defined by $(x_i,$

10 $y_i)$, *A* and *dmax*. This gives the degree of exposure or shelter in the range -1 to 1, where

11 negative values correspond to exposure.

12 To estimate a realistic degree of exposure based on the observed wind pattern at a local site,

13 *Sx* was computed for each of the eight prevailing wind directions *d = [0°, 45°, 90°, 135°,*

14 *180°, 225°, 270°, 315°],* and weighted based on the wind fraction (*wf_d*). *wf_d* accounts for the

15 amount of different exposures in the terrain at various wind directions, and represents the

16 fraction of hourly wind direction observations over the accumulation season for the eight

17 wind directions. The selected period of wind directions influencing the redistribution of snow

18 is January to March. Wind speeds below a threshold of 7 ms^{-1} are excluded, as this threshold

19 is considered a lower limit required for wind drifting of dry snow (Li and Pomeroy, 1997;

20 Lehning and Fierz, 2008). We assume that the snow distribution at snow maximum is highly

21 controlled by the terrain and the general wind exposure over the winter season, and we do not

22 account for the variation in snow properties over the season that controls how much snow is

23 available for transport at a given time.

24 The calculated *Sx* parameter values are used as predictors in different regression analyses to

25 describe the *CV_{sd}* within 1 x 1 km derived from an Airborne Laser Scanning (ALS) of snow

26 depths (see Sect. 4.1). The coefficient of variation of exposure degrees (*CV_{Sx}*) within each *1x1*

27 km grid cell is computed by aggregating the *Sx* map from 10 meter to 1 km resolution

28 according to:

29 $cV_{Sx} = \text{std}(e^{Sx}) / \text{mean}(e^{Sx})$ \qquad (2)

30 *Sx*-values below the 2.5th and above 97.5th percentiles of the *Sx*-distributions are excluded,

31 giving $Sx \approx [-0.2, 0.2]$. Three regression analyses were performed to reduce the RMS between

CV_{Sx} and observed CV_{sd}, where additional predictors such as elevation above treeline (z) and maximum snow depth (μ) have been included (Table 1). Ideally, wind speed should be included as predictor. However, the NORA10 dataset (Section 4.1) does not sufficiently reproduce the local variations in wind speeds over land, especially not at higher elevations and for terrain with increased roughness. Elevation above treeline is chosen as predictor to account for the increased wind exposure with elevation. There is a strong gradient in treeline and general elevation of mountain peaks from high mountains in the south to lower topography in the north of Norway. Therefore, applying only elevation, not adjusted for the local treeline, as predictor would result in an underestimation of redistribution in the north.

3.2 CryoGRID 1 with an integrated sub-grid scheme for snow variation

The equilibrium permafrost model CryoGRID 1 (Gisnås et al., 2013; Westermann et al., 2015) provides an estimate for the *MAGST* (Mean annual ground surface temperature) and *MAGT* (Mean Annual Ground Temperature at the top of the permafrost or at the bottom of the seasonal freezing layer) from freezing (FDD_a) and thawing (TDD_a) degree days in the air according to

$$MAGST = \frac{TDD_a \times nT - FDD_a \times nF}{P} \tag{3}$$

and

$$MAGT = \begin{cases} \dfrac{(TDD_a * nT * r_k - FDD_a * nF)}{P} & \text{for } K_t TDD_s \leq K_f FDD_s \\[2ex] \dfrac{\left(TDD_a * nT - \frac{1}{r_k} * FDD_a * nF\right)}{P} & \text{for } K_t TDD_s \geq K_f FDD_s \end{cases} \tag{4}$$

where P is the period that FDD_a and TDD_a are integrated over, r_k is the ratio of thermal conductivities of the ground in thawed and frozen states (assuming that heat transfer in the ground is entirely governed by heat conduction), while nT and nF are semi-empirical transfer-functions which aim to capture a variety of key processes in one single variable (see Gisnås et al., 2013; Westermann et al., 2015 for details).

The winter nF-factor relates the freezing degree days at the surface to the air and thus accounts for the effect of the winter snow cover, and likewise the nT-factor relates the thawing degree days at the surface to the air and accounts for the surface vegetation cover:

$$FDD_s = nF * FDD_a \quad \text{and} \quad TDD_s = nT * TDD_a \tag{5}$$

1   Variation in observed *n*-factors for forests and shrubs are relatively small, with *nT*-factors

2   typically in the range 0.85 to 1.1, and *nF*-factors in the range 0.3 to 0.5 (Gisnås et al., 2013).

3   Forest, shrubs and mires are assigned *nT*-factors 0.9/1.0/0.85 and *nF*-factors 0.4/0.3/0.6,

4   respectively (Gisnås et al., 2013).

5   Observed variations in *nT* and *nF* within the open non-vegetated areas are comparably large,

6   with values typically in the range $0.4 - 1.2$ for *nT* and $0.1 - 1.0$ for *nF*. The variability is

7   related to the high impact and high spatial variability of snow depths (Gisnås et al., 2014).

8   While *nF* accounts for the insulation from snow due to low thermal conductivity, *nT*

9   indirectly compensates for the shorter season of thawing degree days at the ground surface in

10 areas with a thick snow cover. Relationships between *n*-factors for open areas and maximum

11 snow depths are established based on air and ground temperature observations together with

12 snow depth observations at the end of accumulation season at the 13 stations in southern

13 Norway, presented in Hipp (2012) and at arrays of nearly 80 loggers at Finse and Juvvasshøe

14 (Gisnås et al., 2014) (Fig. 3):

15 $nF = -0.17 * \ln(\mu) + 0.25$ 　　　　　　　　　　　　　　　　　　(6)

16 $nT = -0.13 * \mu + 1.1$ 　　　　　　　　　　　　　　　　　　　　(7)

17 The relationships between *n*-factors and snow cover in open areas are shown to be consistent

18 within the two sites in southern Norway (Gisnås et al., 2014). Due to lack of field

19 observations including all required variables at one site in northern Norway, the relation is not

20 tested for this area. However, it fits very well with a detailed study with 107 loggers recording

21 the variation in ground surface temperature at a lowland site in Svalbard (Gisnås et al. 2014).

22 Other factors, such as solar radiation and soil moisture, have minor effects on the small-scale

23 variation in ground surface temperatures in these areas. Gisnås et al (2014) demonstrated that

24 most of the sub-grid variation in ground temperatures within 1 km x 1 km areas in Norway

25 and Svalbard was reproduced by including only the sub-grid variation of snow depths. In

26 other areas other parameters than snow depth might have a larger effect on the ground surface

27 temperatures, and should be accounted for in the derivation of *n*-factors.

28 We assume that the distribution of maximum snow depths within a grid cell with a given *CV$_{sd}$*

29 and average maximum snow depth (μ) follows a *gamma* distribution with a probability

30 density function (PDF) given by:

1     $f(x; \alpha, \beta) = \frac{1}{\beta^{\alpha} \Gamma(\alpha)} x^{\alpha-1} e^{-\frac{x}{\beta}}$ (8)

2   with a *shape* parameter $\alpha = CV_{sd}^{-2}$ and a *rate* parameter $\beta = \mu * CV_{sd}^{2}$ (e.g. Skaugen et al.,

3   2004; Kolberg and Gottschalk, 2006). The average maximum snow depth corresponds to the

4   coarse scale snow observation, and the original coarse scale snow depth is therefore

5   conserved in the sub-grid snow distribution. Corresponding *n*-factors are computed for all

6   snow depths (*x*) based on Eq. 6 and 7, and related to the PDF (Eq. 8). The model is run for

7   each *nF* from 0 to 1 with 0.01 spacing, giving 100 model realizations. Each realization

8   corresponds to a unique snow depth, represented with a set of *nF* and *nT* factors. Based on the

9   100 realizations, distributions of *MAGST* and *MAGT* are calculated for each grid cell, where

10   the potential permafrost fraction is derived as the percentage of sub-zero *MAGT*. A schematic

11   overview of the model chain and the evaluation is shown in Fig. 4. To assess the sensitivity of

12   the choice of the theoretical distribution function, the model was also run with PDFs

13   following a *lognormal* distribution (e.g. Liston, 2004):

14    $f(x; \lambda, \zeta) = \frac{1}{x\zeta\sqrt{2}} e^{\left\{-\frac{1}{2}\left[\frac{\ln(x)-\lambda}{\zeta}\right]^{2}\right\}}$ (9)

15   where

16    $\lambda = \ln(\mu) - \frac{1}{2}\zeta^{2}, \quad \zeta^{2} = \ln(1 + CV_{sd})$ (10)

17   **3.3   Model evaluation**

18   The CV_{sd} was derived for 0.5 km x 1 km areas based on the ALS snow depth data (Section

19   4.1) resampled to 10 x 10 meter resolution. Each 0.5 x 1 km area includes 500 to 5000 grid

20   cells 10 x 10 m, depending on the area masked out due to lakes or measurement errors. There

21   were > 4000 grid cells in 70% of the areas. Goodness of fit evaluations for the theoretical

22   *lognormal* and *gamma* distributions applying the Anderson-Darling test in MATLAB

23   [adtest.m (Stephens, 1974)] were conducted for each distribution. Parameters for gamma

24   (*shape* and *rate*) and lognormal (*mu*, *sigma*) distributions were estimated by maximum

25   likelihood as implemented in the MATLAB functions gamfit.m and lognfit.m.

26   The results of the permafrost model are evaluated with respect to the average *MAGST* and

27   *MAGT* within each grid cell, as well as the fraction of sub-zero *MAGST*. For the evaluation

28   runs, the model is forced with climatic data for the hydrological year corresponding to the

29   observations. The performance in representing fractional permafrost distribution is evaluated

1 at two field sites where arrays of 26 (Juvvasshøe) and 41 (Finse) data loggers have measured

2 the distribution of ground surface temperatures at 2 cm depth within 500 x 500 meter areas for

3 the hydrological year 2013 (Gisnås et al., 2014). The general lower limits of permafrost are

4 compared to permafrost probabilities derived from BTS (basal temperature of snow) - surveys

5 (Haeberli, 1973; Lewkowicz and Ednie, 2004), conducted at Juvvasshøe and Dovrefjell

6 (Isaksen et al., 2002). The model performance of *MAGST* is evaluated with data from 128

7 temperature data loggers located a few cm below the ground surface in the period 1999 - 2009

8 (Farbrot et al., 2008; Isaksen et al., 2008; Ødegaard et al., 2008; Farbrot et al., 2011; Isaksen

9 et al., 2011; Farbrot et al., 2013). The loggers represent all vegetation classes used in the

10 model and cover spatially large parts of Norway (Fig. 2). Four years of data from 25

11 boreholes (Isaksen et al., 2007; Farbrot et al., 2011; Isaksen et al., 2011; Farbrot et al., 2013)

12 are used to evaluate modelled *MAGT* (Fig. 1). Tables of ground surface temperature loggers

13 (Table S1) and boreholes used for validation (Table S2) are included in the supplementary

14 material.

15

16 **4   Data**

17 **4.1   Forcing and evaluation of the snow distribution scheme**

18 Wind speeds and directions during the snow accumulation season are calculated from the

19 boundary layer wind speed and direction at 10 meter above surface in the Norwegian

20 Reanalysis Archive (NORA10) wind dataset. NORA10 is a dynamically downscaled dataset

21 of ERA -40 to a spatial resolution of 10-11 km, with hourly resolution of wind speed and

22 direction (Reistad et al., 2011). The dataset is originally produced for wind fields over sea,

23 and underestimates the wind speeds at higher elevation over land (Haakenstad et al., 2012).

24 Comparison with weather station data revealed that wind speeds above the tree line are

25 underestimated by about 60% (Haakenstad et al., 2012). For these areas wind speeds in

26 theforcing dataset have been linearly increased by 60 %.

27 The snow distribution scheme is derived from an ALS snow depth over the Hardangervidda

28 mountain plateau in southern Norway (Melvold and Skaugen, 2013). The ALS survey is made

29 along six transects, each covering a 0.5 x 80 km area with nominal 1.5 x 1.5 m ground point

30 spacing. The survey was first conducted between 3rd and 21st of April 2008, and repeated in

31 the period 21st-24th April 2009. The snow cover was at a maximum during both surveys. A

baseline scan was performed 21st of September 2008 to obtain the elevation at minimum snow cover. The ALS data are presented in detail in Melvold and Skaugen (2013). Distributions of snow depth, represented as CV_{sd}, are calculated for each 0.5 x 1 km area, based on the snow depth data resampled to 10 x 10 meter resolution. About 400 cells of 0.5 x 1 km exist for each year, after lakes and areas below treeline are excluded.

The snow distribution scheme is validated with snow depth data obtained by ground penetrating radar (GPR) at Finse (60°34'N, 7°32'E, 1250-1332 m a.s.l.) and Juvvasshøe (61°41'N, 8°23'E, 1374-1497 m a.s.l.). The two field sites are both located in open, non-vegetated alpine landscapes with major wind re-distribution of snow. They differ with respect to mean maximum snow depth (~2 m / ~1 m), average winter wind speeds (7-8 / 10-14 m/s) and topography (very rugged at Finse, while steep, but less rugged at Juvvasshøe). Snow surveys were conducted late March to April (2009, 2012-2014) around maximum snow depth, but when the snow pack was still dry. The GPR surveys at Finse are constrained to an area of 1x1 km, while at Juvvasshøe they cover several square kilometres, but with lower observation density. The GPR data from the end of the accumulation season in 2013 are presented in Gisnås et al. (2014), and the data series from the other years are obtained and processed following the same procedures, described in detail in Dunse et al. (2009). The propagation speed of the radar signal in dry snow was derived from the permittivity and the speed of light in vacuum, with the permittivity obtained from snow density using an empirical relation (Kovacs et al., 1995). The snow depths were determined from the two-way travel time of the reflection from the ground surface and the wave-speed. Observations were averaged over 10 x 10 meter grid cells, where grid cells containing less than three samples were excluded. The CV_{sd} for 1x1 km areas are computed based on the 10-meter resolution data.

4.2 Permafrost model setup

The climatic forcing of the permafrost model is daily gridded air temperature and snow depth data, called the *seNorge* dataset, provided by the Norwegian Meteorological Institute and the Norwegian Water and Energy Directorate. The dataset, available for the period 1961 – 2015, is based on air temperature and precipitation data collected at the official meteorological stations in Norway, interpolated to 1 x 1 km resolution applying Optimal Interpolation as described in Lussana et al. (2010). Snow depths are derived from the air temperature and precipitation data, using a snow algorithm accounting for snow accumulation and melt,

temperature during snow fall and compaction (Engeset et al., 2004; Saloranta, 2012). Freezing- (FDD_a) and thawing (TDD_a) degree days in the air are calculated as annual accumulated negative (FDD) and positive (TDD) daily mean air temperatures, and maximum annual snow depths (μ) are derived directly from the daily gridded snow depth data. The CryoGRID 1 model is implemented at 1 x 1 km resolution over the same grid as the *seNorge* dataset.

Soil properties and surface cover is kept as in Gisnås et al. (2013), with five land cover classes; *forest*, *shrubs*, *open non-vegetated areas*, *mires* and *no data*, based on CLC level 2 in the Norwegian Corine Land Cover map 2012 (Aune-Lundberg and Strand, 2010). Sub-grid distributions of snow are only implemented for *open non-vegetated areas*.

5 Results

5.1 Observed snow distributions in mountain areas of Norway

CV_{sd} within 1 x 1 km areas in the ALS snow survey at Hardangervidda ranged from 0.15 to 1.14, with mean and median of respectively 0.58 and 0.59. According to the Anderson-Darling goodness of fit evaluations 70 out of 932 areas had a snow distribution within the 5% significance interval of a *gamma* distribution, while only 1 area was within the 5% significance interval of a *lognormal* distribution. Although the null hypothesis rejected more than 90% of the sample distributions, the *Anderson-Darling Test Score* was all over lower for the *gamma* distribution, indicating that the observed snow distributions are closer to a *gamma* than to a *lognormal* theoretical distribution (Fig. 5). For lower lying areas with less varying topography and shallower snow depths, in particular in the eastern parts of Hardangervidda, the observed snow distributions were similarly close to both distributions. In higher elevated parts with more snow to the west of the plateau the snow distributions were much closer to a *gamma* distribution. Based on these findings a *gamma* distribution was used in the main model runs, while a model run with *lognormal* distributions of snow was made to evaluate the sensitivity towards the choice of the distribution function (Section 3.2).

5.2 Evaluation of the snow distribution scheme

Three regression models for CV_{sd} as a function of the terrain-based parameter Sx, elevation (z) and mean maximum snow depth (μ) were calibrated with the snow distribution data from the

1   ALS snow survey over the Hardangervidda mountain plateau (Table 1). *Model 1* results in a

2   root mean square error (*RMSE*) of only *0.14*. However, the correlations of the distributions are

3   significantly improved by including *elevation* as predictor (*Model 2; $R^2 = 0.52$*). Including

4   *maximum snow depth* as additional predictor (*Model 3*) the model improves slightly to $R^2 =$

5   0.55 (Fig. 6). The distribution of CV_{sd} (example of *Model 3* in Fig. 8, left) shows increased

6   values in areas of rougher topography (western side of Norway) and higher elevations (central

7   part following the Scandes), with maximum CV_{sd} up to 1.2 in the Lyngen Alps and at peaks

8   around Juvvasshøe (Fig. 1, site 2 and 4). The lowest values of *0.2-0.3* are modelled in larger

9   valleys in south eastern Norway, where elevations are lower and topography gentler.

10   The regression models for CV_{sd} are validated with data from GPR snow surveys at Juvvasshøe

11   and Finse (Table 1). The correlation for *Model 1* is poor, with *$R^2 = 0.04$* and Nash-Sutcliff

12   model efficiency (*ME*) = -0.7 (Table 1). *Model 2* improves the correlation significantly, while

13   the best fit is obtained with *Model 3* (Fig. 6, *RMSE = 0.094*, *$R^2 = 0.62$* and *ME = 0.61*). The

14   improvement in *Model 3* compared to *Model 2* is more pronounced in the validation than in

15   the fit of the regression models, and is mainly a result of better representation of the highest

16   CV_{sd}-values. The validation area at Juvvasshøe is located at higher elevations than what is

17   represented in the ALS snow survey data set and undergoes extreme redistribution by wind.

18   The representation of extreme values, therefore, has a high impact in the validation run.

19   **5.3   Modelled ground temperatures for mainland Norway**

20   The main results presented in this section are based on the model run with 100 realizations per

21   grid cell, applying *gamma* distributions over the CV_{sd} from *Model 3*. The main results are

22   given as averages over the 30-year period 1981 – 2010. According to the model run, in total

23   25 400 km^2 (7.8 %) of the Norwegian mainland is underlain by permafrost in an equilibrium

24   situation with the climate over the 30-years period 1981-2010 (Fig. 1). 12 % of the land area

25   features sub-zero ground temperatures in more than 10% of a 1 km grid cell, and is classified

26   as sporadic (4.4 %), discontinuous (3.2 %) or continuous (4.3 %) permafrost (Fig. 1). In

27   comparison, the model run without a sub-grid variation results in a permafrost area of only

28   13460 km^2, corresponding to 4.1% of the model domain (Table 2). The difference is

29   illustrated for Juvvasshøe (Fig. 7, a) and Dovrefjell (c), where the sub-grid model very well

30   reproduces the observed lower limit of permafrost based on borehole temperatures and BTS-

31   surveys. In contrast, the model without sub-grid variability indicates a hard line for the

1　permafrost limit at much higher elevations (Fig. 7, b and d). At Juvvasshøe, the model without

2　sub-grid distribution still reproduces the permafrost limit to some extent because of the large

3　elevation gradient. At Dovrefjell, where the topography is much gentler, the difference

4　between the models is much larger and the approach without sub-grid distribution is not

5　capable of reproducing the observed permafrost distribution. The modelled permafrost area

6　for model runs applying the other models for CV_{sd} and theoretical distribution functions are

7　summarized in Table 2.

8　The standard deviations of the modelled sub-grid distribution of MAGT range from 0 °C to

9　2.5 °C (Fig. 8, right). The highest *standard deviation* values are found in the Jotunheimen

10　area, where modelled sub-grid variability of MAGT is up to 5 °C. Also at lower elevations in

11　south eastern parts of Finnmark *standard deviations* exceed 1.5 °C. Here, the CV_{sd} values are

12　below 0.4, but because of cold (FDD$_a$ < -2450 °C) and dry (max SD < 0.5 meters) winters

13　even small variations in the snow cover have large effects on the ground temperatures.

14　Close to 70% of the modelled permafrost is situated within open, non-vegetated areas above

15　treeline, classified as mountain permafrost according to Gruber and Haeberli (2009). This is

16　the major part of the permafrost extent both in northern and southern Norway. In northern

17　Norway the model results indicate that the lower limit of continuous and sporadic mountain

18　permafrost decreases eastwards from 1200 and 700 meters a.s.l. in the west, to 500 and 200

19　meters in the east, respectively. In southern Norway, the southernmost location of continuous

20　mountain permafrost is in the mountain massif of Gaustatoppen at 59.8°N, with continuous

21　permafrost above 1700 meters a.s.l. and discontinuous permafrost down to 1200 m a.s.l. In

22　more central southern Norway the continuous mountain permafrost reaches down to 1600

23　meters a.s.l in the western Jotunheimen and Hallingskarvet, and down to 1200 meters a.s.l. in

24　the east at the Swedish border. The sporadic mountain permafrost extends around 200 meters

25　further down both in the western and eastern parts.

26　**5.4 Evaluation of CryoGRID 1 with sub-grid snow distribution scheme**

27　The observed and modelled CV_{sd} values at the field sites were 0.85 and 0.80 at Juvvasshøe,

28　and 0.71 and 0.77 at Finse. At Juvvasshøe the observed fraction of loggers with *MAGST*

29　below 0°C was 77 %, while the model result indicates an aerial fraction of 64 %. Similarly, at

30　Finse the observed negative *MAGST* fraction was 30 %, while the model indicates 32 %. The

31　measured ranges of MAGST within the 1 km x 1 km areas were relatively well reproduced by

1   the model (Table 3). The average MAGST within each field area was also improved

2   compared to a model without a sub-grid representation of snow (Table 3, in parenthesis).

3   58% of the observed *MAGSTs* are captured by the modelled range of *MAGST* for the

4   corresponding grid cell, and 87% within 1°C outside the range given by the distribution. The

5   overall correlation between observed *MAGST* and average modelled *MAGST* for a grid cell is

6   fairly good with *RMSE*, R^2 and *ME* of 1.3°C, 0.65 and 0.37, respectively (Fig. 9, left). The

7   measured *MAGT* was within the range of modelled *MAGT* in all boreholes except one, where

8   *MAGT* deviates 0.2°C outside the range. All the average modelled *MAGT* are within ±1.6°C

9   of observations, while 90 % are within 1°C. The *RMSE* between the observed and modelled

10 average *MAGT* is 0.6°C (Fig. 9, right).

11 The evaluation of the model runs with all three CV_{sd}-models, as well as *lognormal* instead of

12 *gamma* distribution functions are summarized in Table 2. The highest correlation between

13 observed and mean *MAGST* and *MAGT* was obtained by *Model 3*, but *Model 2* yielded similar

14 correlations. All three model runs capture 58 % of the observed *MAGST* and more than 98 %

15 of the observed *MAGT* within the temperature range of the corresponding grid cell. The total

16 area of modelled permafrost is 9% less when applying the simplest snow distribution model

17 (*Model 1*) compared to the reference model (*Model 3*), while the same model without any

18 sub-grid distribution results in 47 % less permafrost area. With a *lognormal* distribution the

19 modelled permafrost area is 18 % less (*Model 3*) than with a *gamma* distribution.

20

21 **6   Discussion**

22 **6.1   The effect of a statistical representation of sub-grid variability in a**
23 **regional permafrost model**

24 The total distribution of modelled permafrost with the sub-grid snow scheme corresponds to

25 7.8% of the Norwegian land area, while the modelled permafrost area without a sub-grid

26 representation of snow only comprises 4%. This large difference in total modelled permafrost

27 area stems exclusively from differences in the amount of modelled permafrost in mountains

28 above the treeline. In these areas the snow distribution is highly asymmetric and a majority of

29 the area have below average snow depths. Because of the non-linearity in the insulating effect

30 of snow cover, the mean ground temperature of a grid cell is not the same as, or even far

from, the ground temperature below the average snow depth. Often, the majority of the area in high, wind exposed mountains is nearly bare blown with most of the snow blown into terrain hollows. Consequently, most of the area experiences significantly lower average ground temperatures than with an evenly distributed, average depth snow cover. In mountain areas with a more gentle topography and relatively small spatial temperature variations, an evenly distributed snow depth will result in large biases in modelled permafrost area, as illustrated at Dovrefjell in Fig. 7. This study provides clear evidence that the sub-grid variability of snow depths should be included in model approaches targeting the ground thermal regime and permafrost distribution.

The model reproduces the large range of variation in sub-grid ground temperatures, with standard deviations up to 2.5 °C, coincident to the observed small-scale variability of up to 6 °C within a single grid cell (Gubler et al., 2011; Gisnås et al., 2014). Inclusion of sub-grid variability of snow depths in the model provides a more adequate representation of the gradual transition from permafrost to permafrost-free areas in alpine environments, and thus a better estimation of permafrost area. In a warming climate, a model without such a sub-grid representation would respond with an abrupt decrease in permafrost extent. In reality, bare blown areas with mean annual ground temperatures of -6 °C need a large temperature increase to thaw. Increased precipitation as snow would also warm the ground; however, bare blown areas may still be bare blown with increased snow accumulation during winter. A statistical snow distribution reproduces this effect, also with an increase in mean snow depth.

CryoGRID1 is a simple modelling scheme delivering a mean annual ground temperature at the top of the permanently frozen ground based on near-surface meteorological variables, under the assumption that the ground thermal regime is in equilibrium with the applied surface forcing. This is a simplification, and the model cannot reproduce the transient evolution of ground temperatures, and is therefore not suitable for future climate predictions. However, it has proven to capture the regional patterns of permafrost reasonably well (Gisnås et al., 2013; Westermann et al., 2013). Because of the simplicity it is computationally efficient, and suitable for doing test-studies like the one presented in this paper and in similar studies (Westermann et al., 2015).

For the model evaluation with measured ground temperatures in boreholes (Section 5.4), the modelled temperatures are forced with data for the hydrological year corresponding to the observations. Because of the assumption of an equilibrium situation in the model approach,

1 such a comparison can be problematic as many of the boreholes have undergone warming

2 during the past decades. However, with the majority of the boreholes located in bedrock or

3 coarse moraine material with relatively high conductivity, the lag in the climate signal is

4 relatively small at the top of the permafrost. The lag will also vary from borehole to borehole,

5 depending on the ground thermal properties. Since we use data distributed over larger areas

6 and longer time periods, including a large range of situations, the effect is mainly evident in

7 terms of a larger statistical spread and not a systematic error.

8 The large amount of field observations used for calibration and evaluation in this study is

9 mainly conducted in alpine mountain areas. The large spatial variation in winter snow depths

10 is a major controlling factor also of the ground temperatures in peat plateaus and palsa mires,

11 and is a driving factor in palsa formation (Seppälä, 2011). The sub-grid effect of snow should

12 therefore also be implemented for mire areas, where comparable data sets are lacking.

6.2 Model sensitivity

14 The sensitivity of CV_{sd}-model to the modelled ground temperatures is relatively low, with

15 only 9 % variation in permafrost area, although the performance of the snow distribution

16 scheme varies significantly between the models when evaluated with GPR snow surveys

17 (Table 1). In comparison, a *lognormal* instead of a *gamma* distribution function reduces the

18 permafrost area by 18% (Table 2). The choice of distribution function therefore seems to be

19 of greater importance than the fine tuning of a model for CV_{sd}. This result contradicts the

20 conclusions by Luce and Tarboton (2004), which suggest that the parameterization of the

21 distribution function is more important than the choice of distribution model. With a focus on

22 hydrology and snow cover depletion curves, equal importance was given to both the deeper

23 and shallower snow depths in the mentioned study. In contrast, an accurate representation of

24 the shallowest snow depths is crucial for modelling the ground thermal regime. The low

25 thermal conductivity of snow results in a disconnection of ground surface and air

26 temperatures at snow packs thicker than $0.5 - 1$ m, depending on the physical properties of

27 the snow pack and the surface roughness (Haeberli, 1973). In wind exposed areas prone to

28 heavy redistribution, large fractions of the area will be entirely bare blown (Gisnås et al.,

29 2014). These are the areas of greatest importance for permafrost modelling. In order to

30 reproduce the gradual transition in the discontinuous permafrost zone, where permafrost is

31 often only present at bare blown ridges, shallow snow covers must be satisfactorily

represented. Compared to a *gamma* function, a *lognormal* distribution function to a larger degree underestimates the fraction of shallow snow depths, resulting in a less accurate representation of this transition.

Several studies include statistical representations of the sub-grid variability of snow in hydrological models, most commonly applying a two- or three-parameter *lognormal* distribution (e.g. Donald et al., 1995; Liston, 2004; Pomeroy et al., 2004; Nitta et al., 2014). Observed snow distributions within 1x1 km in the ALS snow survey presented in this paper are closer to a *gamma* than to a *lognormal* distribution, supporting the findings by Skaugen (2007) and Winstral and Marks (2014) which were both conducted in non-forested alpine environments. However, the difference is not substantial in all areas; the two distributions can provide near-equal fit in eastern parts of the mountain plateau where the terrain is gentler and the wind speeds are lower. We suggest that the choice of distribution function of snow is important in model applications for the ground thermal regime, and recommend the use of *gamma* distribution for non-vegetated high alpine areas prone to heavy redistribution of snow.

While a *gamma* distribution offers improvements over a *lognormal* distribution, the bare blown areas are still not sufficiently represented. One attempt to solve this is to include a third parameter for the "snow free fraction" (e.g. Kolberg et al., 2006; Kolberg and Gottschalk, 2010). We made an attempt to calibrate such a parameter for this study, however, no correlations to any of the predictors were found. It is also difficult to determine a threshold depth for "snow free" areas in ALS data resampled to 10 meter resolution, where the uncertainty of the snow depth observations are in the order of ten centimetres (Melvold and Skaugen, 2013).

In this study a high number of realizations could be run per grid cell because of the low computational cost of the model. To evaluate the sensitivity of sampling density, the number of realizations was reduced from 100 to 10 per grid cell. This resulted is a 2.6 % increase in total modelled permafrost area relative to the reference model run. This demonstrates that a statistical downscaling of ground temperatures as demonstrated in this study is robust and significantly improves the model results with only a few additional model realizations per grid cell.

7 Conclusions

We present a modelling approach to reproduce the variability of ground temperatures within the scale of 1 km^2 grid cells based on probability distribution functions over corresponding seasonal maximum snow depths. The snow distributions are derived from climatic parameters and terrain parameterizations at 10 meter resolution, and are calibrated with a large scale data set of snow depths obtained from laser scanning. The model results are evaluated with independent observations of snow depth distributions, ground surface temperature distributions and ground temperatures. From this study the following conclusions can be drawn:

- The total modelled permafrost area in an equilibrium with the average climate for the period 1981 – 2010 is 25 400 km^2. This corresponds to 7.8 % of the Norwegian mainland.

- The model simulation without a sub-grid representation of snow produces almost 50 % less permafrost.

- Due to the non-linear insulating effect of snow in combination with asymmetric snow distributions within each grid cell, the spatial average ground temperature in a 1km² area cannot be determined based on the average snow cover for that area.

- Observed variations in ground surface temperatures from two logger arrays with 26 and 41 loggers, respectively, are very well reproduced, with estimated fractions of sub-zero *MAGST* within ±10%.

- 94 % of the observed mean annual temperature at top of permafrost in the boreholes are within the modelled ground temperature range for the corresponding grid cell, and mean modelled temperature of the grid cell reproduces the observations with an accuracy of 1.5°C or better.

- The sensitivity of the model to the coefficient of variation of snow (CV_{sd}) is relatively low, compared to the choice of theoretical snow distribution function. Both are minor effects compared to the effect of running the model without a sub-grid distribution.

- The observed CV_{sd} of snow within 1 km^2 grid cells in the Hardangervidda mountain plateau varies from 0.15 to 1.15, with an average CV_{sd} of 0.6. The observed CV_{sd} values are nearly identical at the end of the accumulation seasons in 2008 and 2009.

- The distributions are generally closer to a theoretical *gamma* distribution than to a *lognormal* distribution, in particular in areas of very rough topography, thicker snow cover and higher average winter wind speeds.

In areas subject to snow redistribution, the average ground temperature of a 1 km^2 grid cell must be determined based on the distribution, and not the overall average of snow depths within the grid cell. Modelling the full range of ground temperatures present over small distances facilitates a better representation of the gradual transition from permafrost to non-permafrost areas and most likely a more accurate response to climate warming. This study demonstrates that accounting for the sub-grid variability of snow depths can strongly improve model estimates of the ground thermal regime and permafrost distribution alpine conditions.

References

Aune-Lundberg, L., and Strand, G.-H.: CORINE Land Cover 2006. The Norwegian CLC2006 project, Report from the Norwegian Forest and Landscape Institute: 11/10, 14p, 2010.

Clark, M. P., Hendrikx, J., Slater, A. G., Kavetski, D., Anderson, B., Cullen, N. J., Kerr, T., Hreinsson, E. Ö., and Woods, R. A.: Representing spatial variability of snow water equivalent in hydrologic and land-surface models: A review, Water Resources Research, 47, 10.1029/2011WR010745, 2011.

Donald, J. R., Soulis, E. D., Kouwen, N., and Pietroniro, A.: A Land Cover-Based Snow Cover Representation for Distributed Hydrologic Models, Water Resources Research, 31, 995-1009, 10.1029/94WR02973, 1995.

Dunse, T., Schuler, T. V., Hagen, J. O., Eiken, T., Brandt, O., and Høgda, K. A.: Recent fluctuations in the extent of the firn area of Austfonna, Svalbard, inferred from GPR, Annals of Glaciology, 50, 155-162, 10.3189/172756409787769780, 2009.

Engeset, R., Tveito, O. E., Alfnes, E., Mengistu, Z., Udnæs, C., Isaksen, K., and Førland, E. J.: Snow map System for Norway., XXIII Nordic Hydrological Conference, 8-12 Aug., Tallin, Estonia. NHP Report: 48(1), 2004,

Farbrot, H., Isaksen, K., and Etzelmüller, B.: Present and past distribution of mountain permafrost in Gaissane Mountains, Northern Norway, In: Proceeding of the Ninth International Conference on Permafrost, Fairbanks, Alaska, 2008, 427–432,

Farbrot, H., Hipp, T. F., Etzelmüller, B., Isaksen, K., Ødegård, R. S., Schuler, T. V., and Humlum, O.: Air and Ground Temperature Variations Observed along Elevation and Continentality Gradients in Southern Norway, Permafrost and Periglacial Processes, 22, 343-360, 10.1002/ppp.733, 2011.

Farbrot, H., Isaksen, K., Etzelmüller, B., and Gisnås, K.: Ground Thermal Regime and Permafrost Distribution under a Changing Climate in Northern Norway, Permafrost and Periglacial Processes, 24, 20-38, 10.1002/ppp.1763, 2013.

Fiddes, J., and Gruber, S.: TopoSUB: a tool for efficient large area numerical modelling in complex topography at sub-grid scales, Geosci. Model Dev., 5, 1245-1257, 10.5194/gmd-5-1245-2012, 2012.

Gisnås, K., Etzelmuller, B., Farbrot, H., Schuler, T. V., and Westermann, S.: CryoGRID 1.0: Permafrost Distribution in Norway estimated by a Spatial Numerical Model, Permafrost and Periglacial Processes, 24, 2-19, 10.1002/ppp.1765, 2013.

Gisnås, K., Westermann, S., Schuler, T. V., Litherland, T., Isaksen, K., Boike, J., and Etzelmüller, B.: A statistical approach to represent small-scale variability of permafrost temperatures due to snow cover, The Cryosphere, 8, 2063-2074, 10.5194/tc-8-2063-2014, 2014.

Goodrich, L. E.: The influence of snow cover on the ground thermal regime, Can. Geotech. J., 19, 421-432, 1982.

Gruber, S., and Haeberli, W.: Mountain permafrost, in: Permafrost Soils, edited by: Margesin, R., Springer, 33-44, 2009.

Gubler, H., Fiddes, J., Gruber, S., and Keller, M.: Scale-dependent measurement and analysis of ground surface temperature variability in alpine terrain, The Cryosphere, 5, 307-338, 10.5194/tcd-5-307-2011, 2011.

Haakenstad, H., Reistad, M., Haugen, J. E., and Breivik, Ø.: Update of the NORA10 hindcast archive for 2011 and study of polar low cases with the WRF model, met.no report 17/2012, Oslo, 2012.

Haeberli, W.: Die Basis-Temperatur der winterlichen Schneedecke als möglicher Indikator für die Verbreitung von Permafrost in den Alpen, Zeitschrift für Gletscherkunde und Glazialgeologie, 9, 221-227, 1973.

Hipp, T.: Mountain Permafrost in Southern Norway. Distribution, Spatial Variability and Impacts of Climate Change., PhD, Faculty of Mathematics and Natural Sciences, Department of Geosciences, University of Oslo, 166 pp., 2012.

Isaksen, K., Hauck, C., Gudevang, E., Ødegård, R. S., and Sollid, J. L.: Mountain permafrost distribution in Dovrefjell and Jotunheimen, southern Norway, based on BTS and DC resistivity tomography data, Norsk Geografisk Tidsskrift-Norwegian Journal of Geography, 56, 122-136, 10.1080/002919502760056459, 2002.

Isaksen, K., Sollid, J. L., Holmlund, P., and Harris, C.: Recent warming of mountain permafrost in Svalbard and Scandinavia, Journal of Geophysical Research., 112, F02S04, 10.1029/2006jf000522, 2007.

Isaksen, K., Farbrot, H., Blikra, L., Johansen, B., Sollid, J., and Eiken, T.: Five year ground surface temperature measurements in Finnmark, Northern Norway., Ninth International Conference on Permafrost, Fairbanks, Alaska, 2008, 789–794,

Isaksen, K., Ødegård, R. S., Etzelmüller, B., Hilbich, C., Hauck, C., Farbrot, H., Eiken, T., Hygen, H. O., and Hipp, T. F.: Degrading Mountain Permafrost in Southern Norway: Spatial and Temporal Variability of Mean Ground Temperatures, 1999–2009, Permafrost and Periglacial Processes, 22, 361-377, 10.1002/ppp.728, 2011.

Kolberg, S., Rue, H., and Gottschalk, L.: A Bayesian spatial assimilation scheme for snow coverage observations in a gridded snow model, Hydrol. Earth Syst. Sci., 10, 369-381, 10.5194/hess-10-369-2006, 2006.

Kolberg, S., and Gottschalk, L.: Interannual stability of grid cell snow depletion curves as estimated from MODIS images, Water Resources Research, 46, n/a-n/a, 10.1029/2008WR007617, 2010.

Kolberg, S. A., and Gottschalk, L.: Updating of snow depletion curve with remote sensing data, Hydrological Processes, 20, 2363-2380, 2006.

Kovacs, A., Gow, A. J., and Morey, R. M.: The in-situ dielectric constant of polar firn revisited, Cold Regions Science and Technology, 23, 245-256, 10.1016/0165-232X(94)00016-Q, 1995.

Langer, M., Westermann, S., Heikenfeld, M., Dorn, W., and Boike, J.: Satellite-based modeling of permafrost temperatures in a tundra lowland landscape, Remote Sensing of Environment, 135, 12-24, 10.1016/j.rse.2013.03.011, 2013.

Lehning, M., and Fierz, C.: Assessment of snow transport in avalanche terrain, Cold Regions Science and Technology, 51, 240-252, 10.1016/j.coldregions.2007.05.012, 2008.

Lewkowicz, A. G., and Ednie, M.: Probability mapping of mountain permafrost using the BTS method, Wolf Creek, Yukon Territory, Canada, Permafrost and Periglacial Processes, 15, 67-80, 10.1002/ppp.480, 2004.

Li, L., and Pomeroy, J. W.: Estimates of Threshold Wind Speeds for Snow Transport Using Meteorological Data, Journal of Applied Meteorology, 36, 205-213, 10.1175/1520-0450(1997)036<0205:EOTWSF>2.0.CO;2, 1997.

Liston, G. E.: Representing Subgrid Snow Cover Heterogeneities in Regional and Global Models, Journal of Climate, 17, 1381-1397, 10.1175/1520-0442(2004)017<1381:RSSCHI>2.0.CO;2, 2004.

Luce, C. H., and Tarboton, D. G.: The application of depletion curves for parameterization of subgrid variability of snow, Hydrological Processes, 18, 1409-1422, 10.1002/hyp.1420, 2004.

Lussana, C., Uboldi, F., and Salvati, M. R.: A spatial consistency test for surface observations from mesoscale meteorological networks, Quarterly Journal of the Royal Meteorological Society, 136, 1075-1088, 10.1002/qj.622, 2010.

Melvold, K., and Skaugen, T.: Multiscale spatial variability of lidar-derived and modeled snow depth on Hardangervidda, Norway, Annals of Glaciology, 54, 273-281, 10.3189/2013AoG62A161, 2013.

Nitta, T., Yoshimura, K., Takata, K., O'ishi, R., Sueyoshi, T., Kanae, S., Oki, T., Abe-Ouchi, A., and Liston, G. E.: Representing Variability in Subgrid Snow Cover and Snow Depth in a Global Land Model: Offline Validation, Journal of Climate, 27, 3318-3330, 10.1175/JCLI-D-13-00310.1, 2014.

Pomeroy, J., Essery, R., and Toth, B.: Implications of spatial distributions of snow mass and melt rate for snow-cover depletion: observations in a subarctic mountain catchment, Annals of Glaciology, 38, 195-201, 10.3189/172756404781814744, 2004.

Reistad, M., Breivik, Ø., Haakenstad, H., Aarnes, O. J., Furevik, B. R., and Bidlot, J.-R.: A high-resolution hindcast of wind and waves for the North Sea, the Norwegian Sea, and the Barents Sea, Journal of Geophysical Research: Oceans, 116, C05019, 10.1029/2010JC006402, 2011.

Saloranta, T. M.: Simulating snow maps for Norway: description and statistical evaluation of the seNorge snow model, The Cryosphere, 6, 1323-1337, 10.5194/tc-6-1323-2012, 2012.

Seppälä, M.: Synthesis of studies of palsa formation underlining the importance of local environmental and physical characteristics, Quaternary Research, 75, 366-370, http://dx.doi.org/10.1016/j.yqres.2010.09.007, 2011.

Skaugen, T., Alfnes, E., Langsholt, E. G., and Udnæs, H.-C.: Time-variant snow distribution for use in hydrological models, Annals of Glaciology, 38, 180-186, 10.3189/172756404781815013, 2004.

Skaugen, T.: Modelling the spatial variability of snow water equivalent at the catchment scale, Hydrol. Earth Syst. Sci., 11, 1543-1550, 10.5194/hess-11-1543-2007, 2007.

Stephens, M. A.: EDF Statistics for Goodness of Fit and Some Comparisons, Journal of the American Statistical Association, 69, 730-737, 10.1080/01621459.1974.10480196, 1974.

Westermann, S., Schuler, T. V., Gisnås, K., and Etzelmüller, B.: Transient thermal modeling of permafrost conditions in Southern Norway, The Cryosphere, 7, 719-739, 10.5194/tc-7-719-2013, 2013.

Westermann, S., Østby, T., Gisnås, K., Schuler, T. V., and Etzelmüller, B.: A ground temperature map of the North Atlantic permafrost region based on remote sensing and reanalysis data, The Cryosphere, 9, 1303-1319, 10.5194/tc-9-1303-2015, 2015.

Winstral, A., Elder, K., and Davis, R. E.: Spatial snow modeling of wind-redistributed snow using terrain-based parameters, Journal of Hydrometeorology, 3, 524-538, http://dx.doi.org/10.1175/1525-7541(2002)003<0524:SSMOWR>2.0.CO;2, 2002.

Winstral, A., and Marks, D.: Long-term snow distribution observations in a mountain catchment: Assessing variability, time stability, and the representativeness of an index site, Water Resources Research, 50, 293-305, 10.1002/2012WR013038, 2014.

Zhang, T., Barry, R. G., and Haeberli, W.: Numerical simulations of the influence of the seasonal snow cover on the occurrence of permafrost at high latitudes, Norsk Geografisk

Tidsskrift - Norwegian Journal of Geography, 55, 261-266, 10.1080/00291950152746621, 2001.

Ødegaard, R. S., Isaksen, K., Eiken, T., and Sollid, J. L.: MAGST in Mountain Permafrost, Dovrefjell, Southern Nroway, 2001-2006, Ninth International Conference on Permafrost (NICOP) 2008, Fairbanks, Alaska, June 29 - July 3, 2008.

Figures:
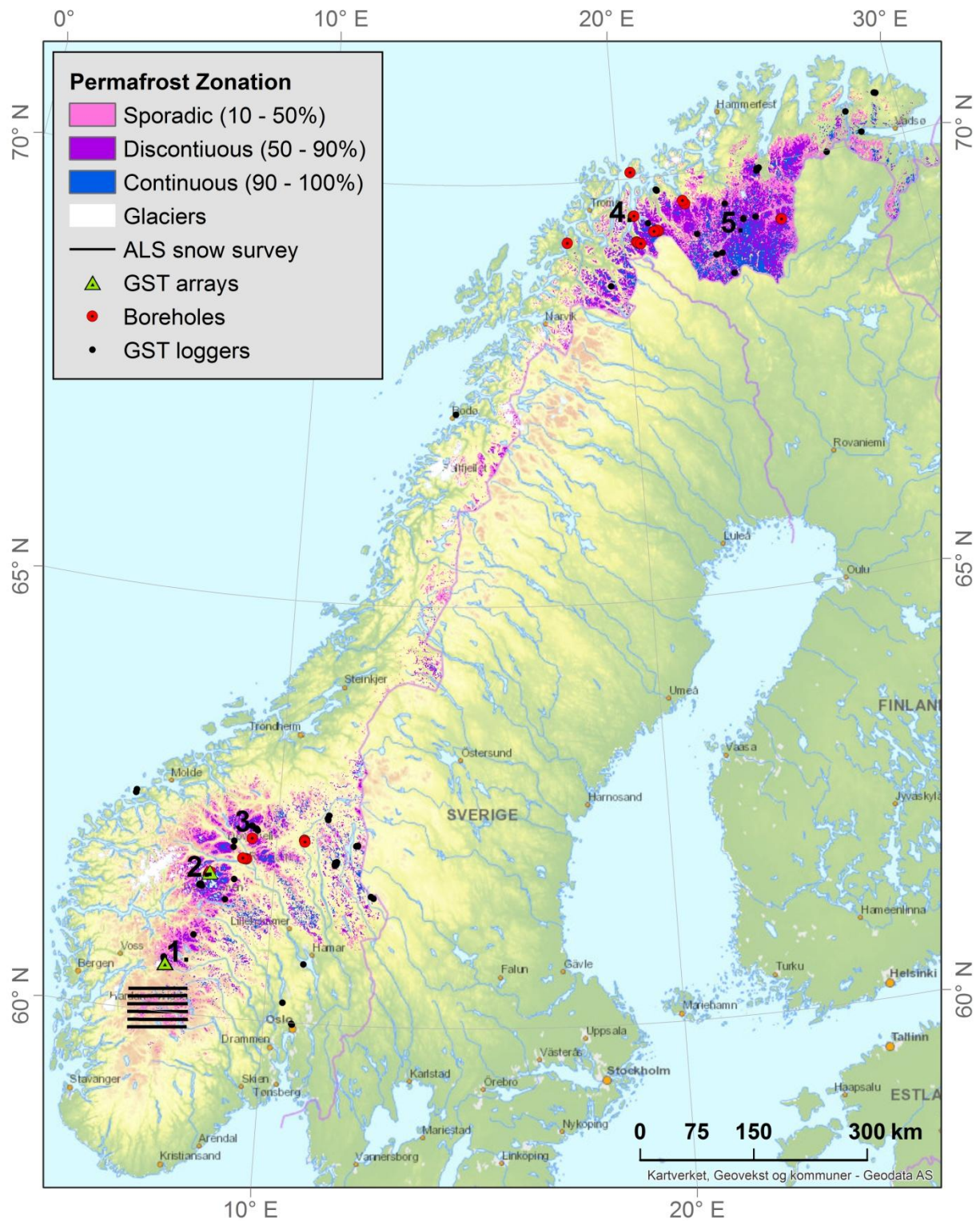
3   Fig. 1: Modelled distribution of permafrost in Norway. Sites mentioned in the text: 1) Finse,

4   south of Hallingskarvet, 2) Juvvasshøe in Jotunheimen, 3) Dovrefjell, 4) The Lyngen Alps

5   and 5) Finnmark.

1
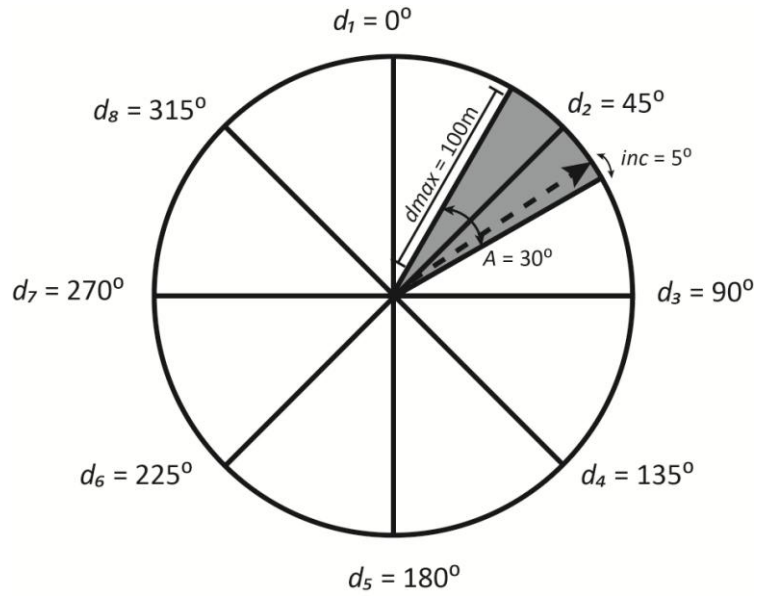
2

3   Fig. 2: The area accounted for in each of the 8 runs of the Winstral terrain-based parameter,

4   each of them with a prevailing wind direction d_n. The area accounted for when calculating the

5   exposure of a grid cell is constrained by the search window (A) and the search distance *dmax*

6   being 100 meters upwind.

7
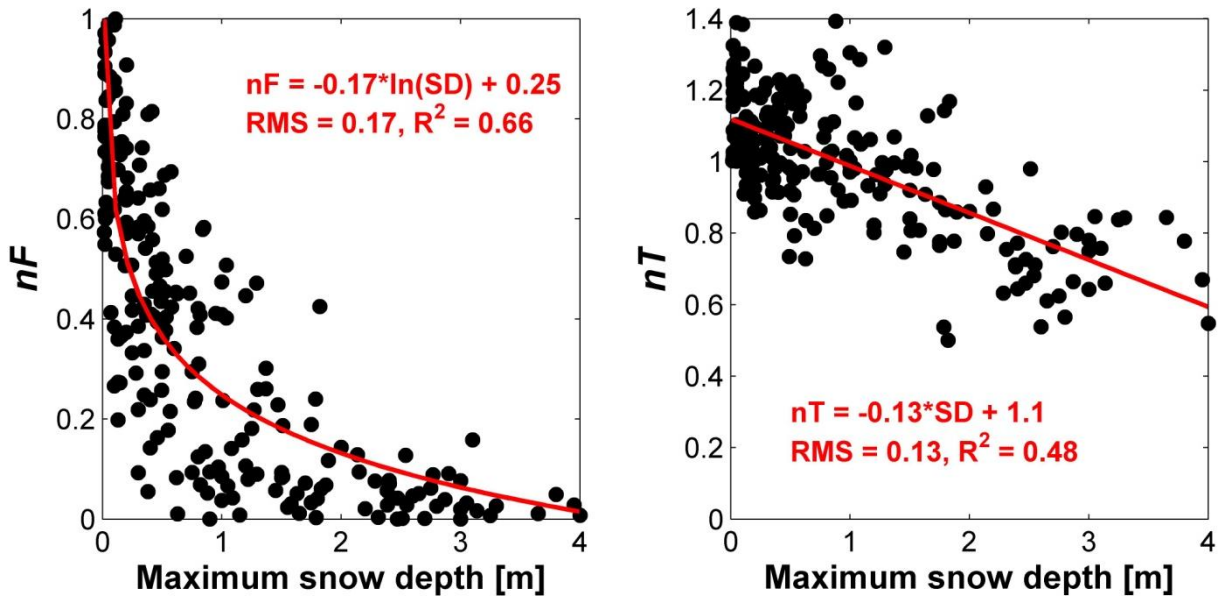
8

9   Fig. 3: *nF* and *nT* related to maximum snow depth observed at more than 90 sites located

10   above 1000 m a.s.l. in southern Norway.

INPUT MODEL EVALUATION

DTM (10 m res)	Sub-grid snow routine *Output: CV*	Calibration ALS snow depth data
Wind data (0.5° res)		Evaluation GPR snow depth data
Snow depths	CryoGRID 1 *Output: MAGST and MAGT*	Calibration of *n*-factors GST-logger arrays
Air temperatures		Evaluation MAGST: distributed GST loggers MAGT: borehole data
CORINE land cover		
Sediment cover		

1
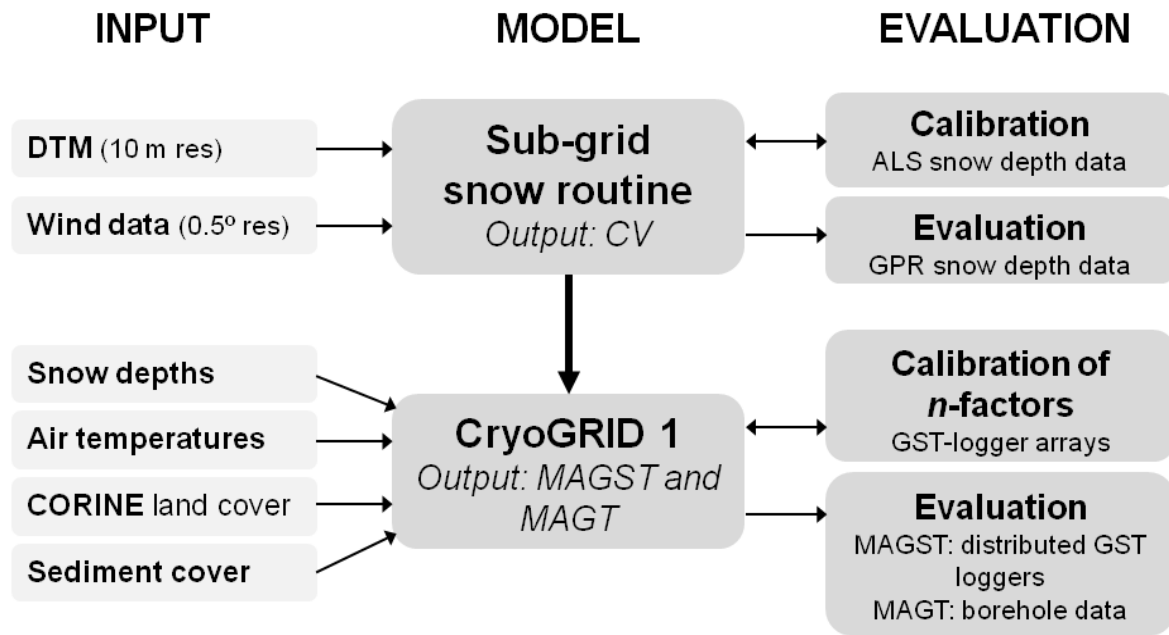
2   Fig. 4: Schematic of the model chain, including input data, calibration and evaluation

3   procedures.

4
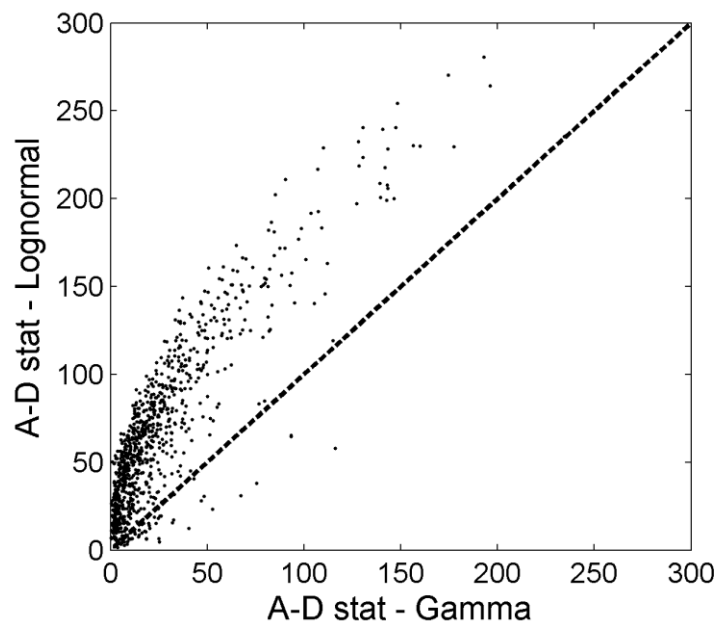
5   Fig. 5: Scores from the Anderson-Darling test statistics for Goodness-of-Fit between

6   theoretical *gamma* and *lognormal* distributions and the observed distribution within each 1x1

7   km area in the ALS snow survey. Lower scores indicate better fit.

8

1
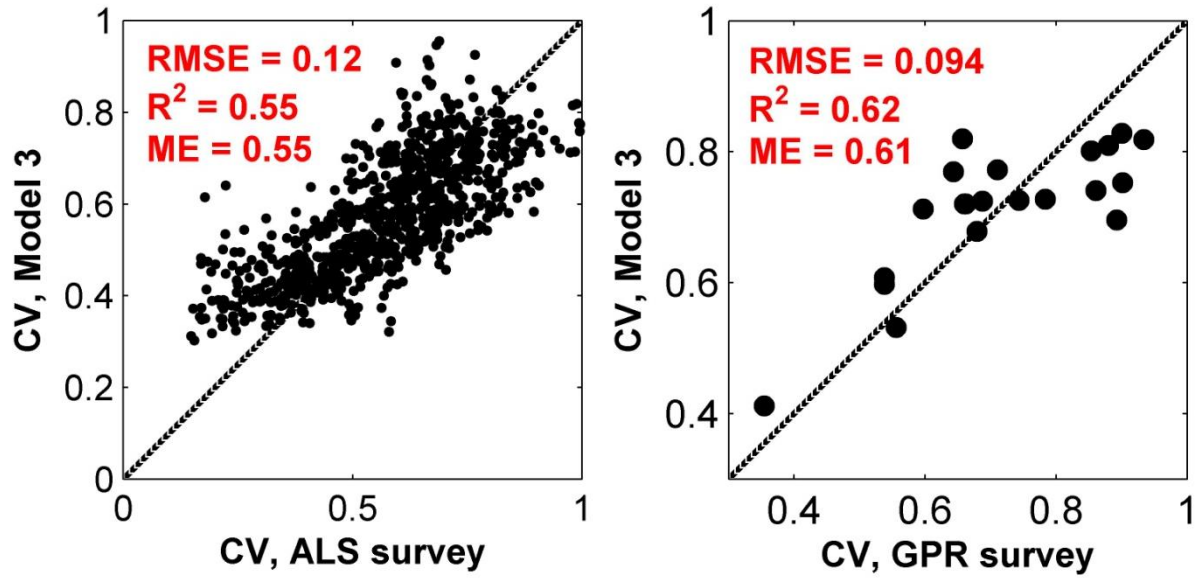
Fig. 6: Left: Fit of the regression *Model 3* for CV_{sd}, calibrated with CV_{sd} derived from the ALS snow survey. Right: The model performance is evaluated with independent ground penetrating radar (GPR) snow surveys from at Finse and Juvvasshøe.
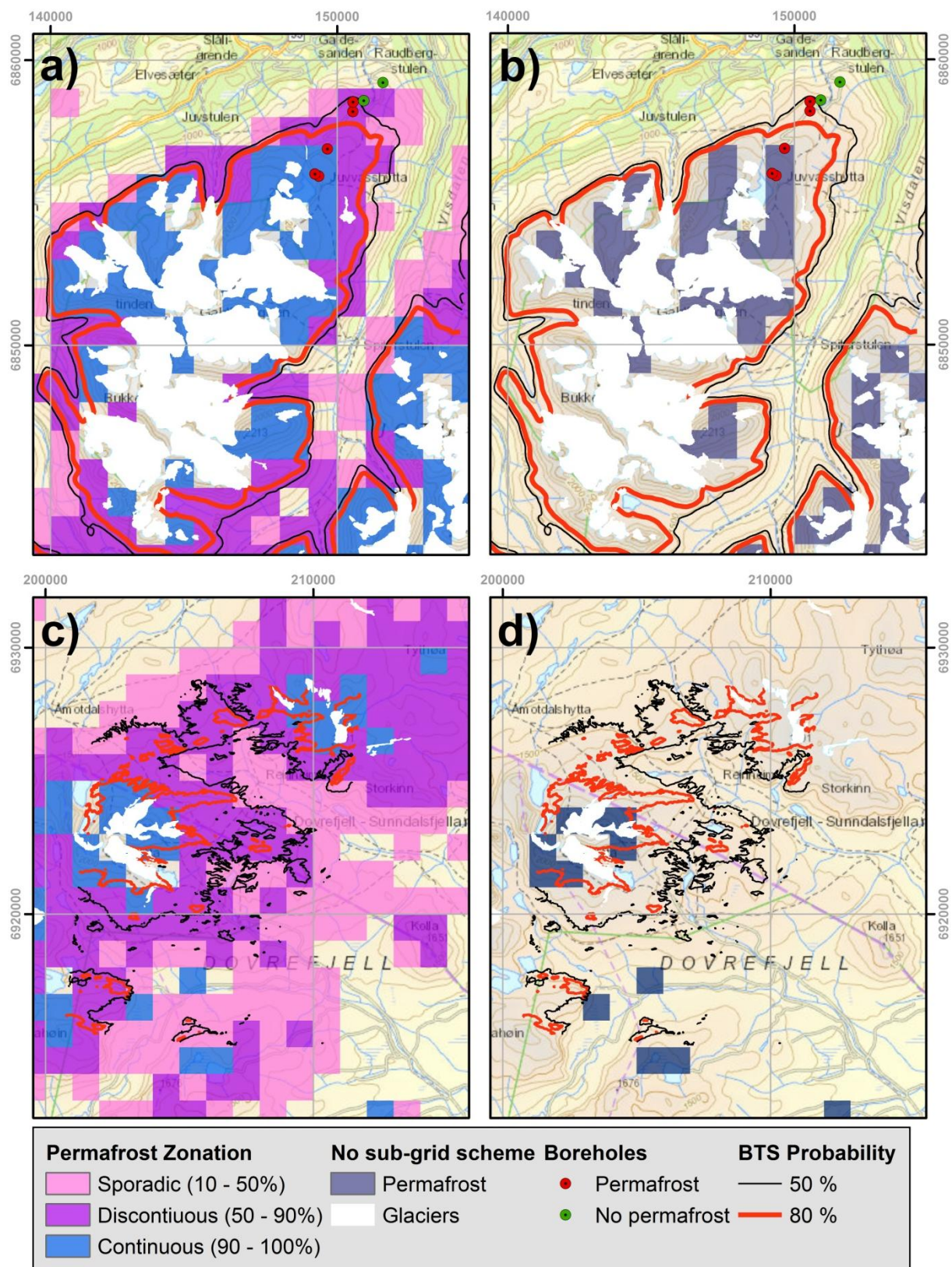
Fig. 7: Distribution of permafrost at Juvvasshøe in Jotunheimen (a and b), and at Dovrefjell (c and d) modelled as permafrost zones applying the sub-grid approach (left) compared to the modelled mean annual ground temperature (*MAGT*) without a sub-grid approach (right).

1 Lower limit of 50 % and 80 % probability of permafrost derived from BTS-surveys are shown

2 as black and red contour lines, respectively. Borehole locations with permafrost (red) and

3 seasonal frost (green) are shown as dots in the map at Juvvasshøe.

4

5
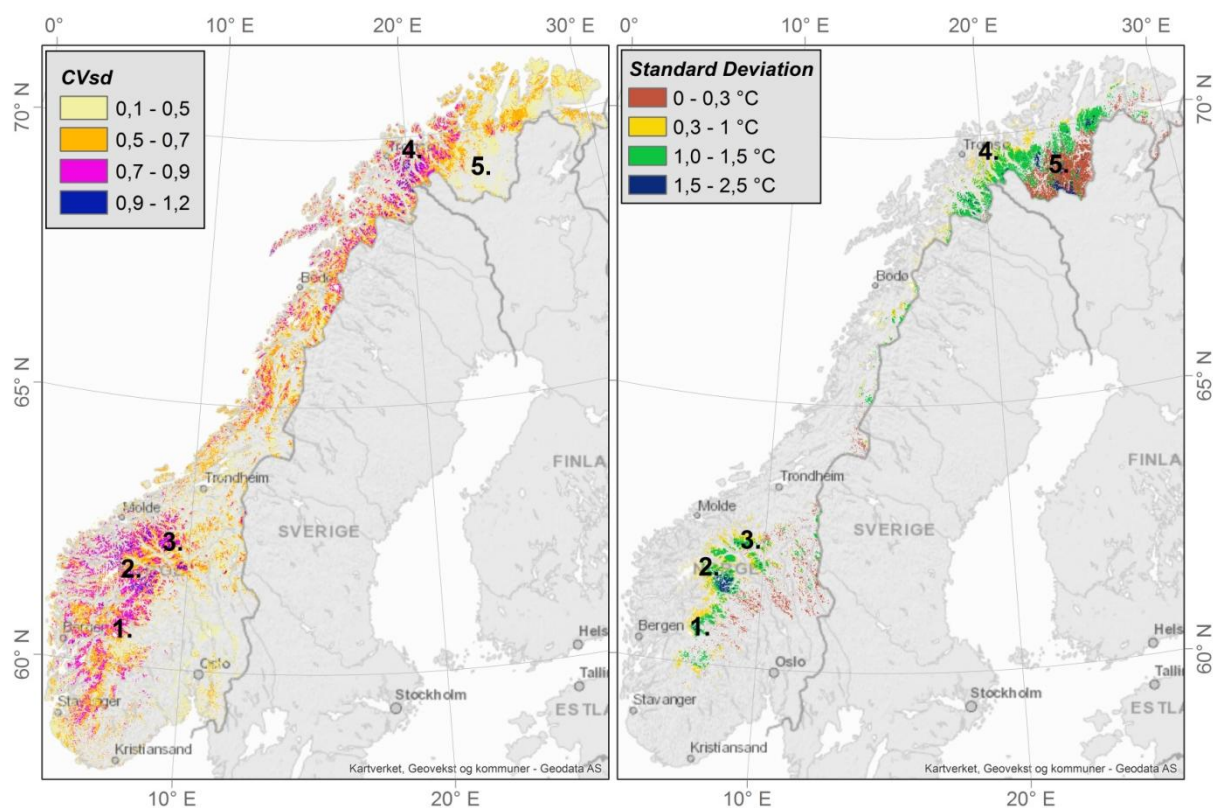
6 Fig. 8: Left: Distribution of modelled CV_{sd} in non-vegetated areas of Norway with *Model 3*.

7 CV_{sd} increases in areas of rougher topography (western side of Norway) and higher elevations

8 (central part following the Scandes). Right: Standard deviation of modelled *MAGT* for areas

9 of modelled permafrost. Sites mentioned in the text: 1) Finse, south of Hallingskarvet, 2)

10 Juvvasshøe in Jotunheimen, 3) Dovrefjell, 4) The Lyngen Alps and 5) Finnmark.

11
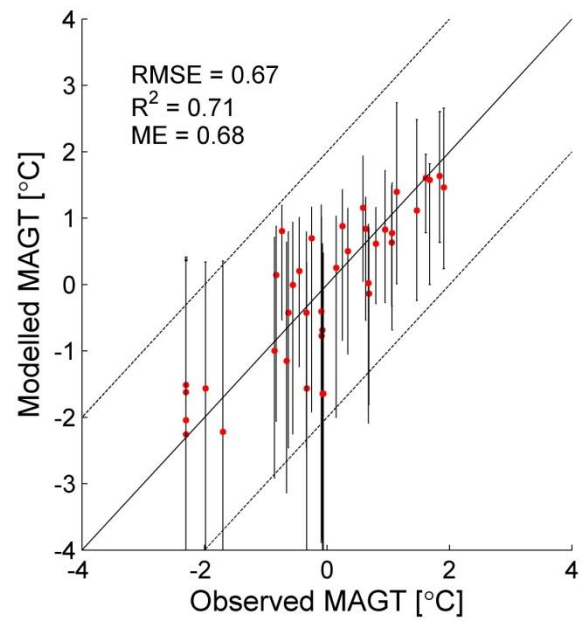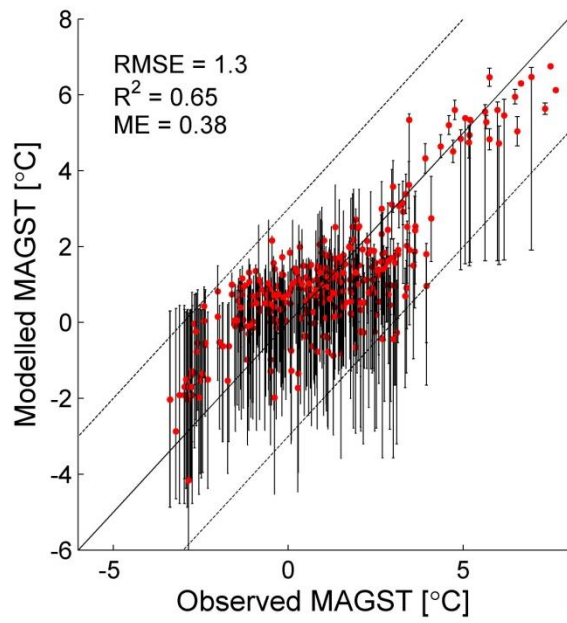
Fig. 9: Correlation between modelled and observed *MAGST* (left) and *MAGT* at the top of permafrost (right). The dotted line indicates ± 2 °C of the 1:1 line (black line). The vertical bars indicate the variation of modelled temperatures within the grid cell, and the red dots indicates the mean temperature.

1 **Tables:**

2 Table 1: The three regression models for CV_{sd} with in increasing number of predictors are

3 calibrated with observed snow distributions from the ALS snow survey (left columns). P-

4 values are $< 10^{-6}$. The isolated snow distribution scheme is validated with independent snow

5 distribution data collected with GPR snow surveys (right columns). Root mean square error

6 ($RMSE$), coefficient of determination (R^2) and Nash-Sutcliffe model efficiency (ME) are

7 given for each model evaluation.

8	$CV_{sd} =$	Fit of regression			CV_{sd}, GPR survey		
		RMSE	R^2	ME	RMSE	R^2	ME
Model 1	$0.39 + 3.4*CV_{Sx}$	0.14	0.36	0.36	0.20	0.04	-0.71
Model 2	$0.31 + 3.1*CV_{Sx} + 4.05\text{e-}4*z$	0.12	0.52	0.52	0.12	0.59	0.36
Model 3	$0.40 + 3.1*CV_{Sx} + 4.95\text{e-}04*z - 0.0713*\mu$	0.12	0.55	0.55	0.09	0.62	0.61

8

9 Table 2: The model performance is evaluated with respect to the mean annual ground surface

10 temperatures ($MAGST$) and the mean annual temperature at the depth of the active layer or

11 seasonal freezing layer ($MAGT$). Modelled average $MAGST$ or $MAGT$ over a grid cell is

12 compared to more than 100 GST logger locations and 25 boreholes. The location of the GST

13 loggers and boreholes are shown in Fig. 1. Modelled permafrost distribution is given in total

14 areas, and as percentage of the model domain, corresponding to the Norwegian mainland area.

		Permafrost model evaluation						Modelled permafrost area	
		MAGST, GST loggers			MAGT, boreholes				
		RMSE	R^2	ME	RMSE	R^2	ME	[km^2]	[%]
No sub-grid variation		1.57	0.65	-0.56	1.19	0.62	-1.90	13 462	4.1
GAMMA	CV_{sd} = 0.6	1.37	0.64	0.06	0.77	0.66	0.22	23 571	7.3
	Model 1	1.36	0.63	0.12	0.77	0.66	0.11	23 147	7.1
	Model 2	1.29	0.65	0.31	0.65	0.71	0.62	23 674	7.3
	Model 3*	**1.29**	**0.65**	**0.38**	**0.67**	**0.71**	**0.68**	**25 407**	**7.8**
LOGN	Model 1	1.40	0.64	-0.06	0.87	0.67	-0.25	19 975	6.2
	Model 2	1.38	0.65	0.01	0.82	0.69	0.09	20 067	6.2
	Model 3	1.36	0.65	0.06	0.78	0.69	0.22	20 889	6.2

15 *Reference model run.

16

17

18

1 Table 3: Observed and modelled values for the coefficient of variation for maximum snow
2 depth (CV_{sd}) and spatial distributions of Mean Annual Ground Surface Temperatures
3 (MAGST) at the field sites at Finse and Juvvasshøe. The MAGST modelled without a sub-
4 grid distribution of snow is given in parenthesis.

	Juvvasshøe		Finse	
	Observed	Modelled	Observed	Modelled
CV_{sd}	0.85	0.80	0.71	0.77
MAGST < 0 °C	77 %	64 %	30 %	32 %
$MAGST_{min}$	-1.8 °C	-2.6 °C	-1.9 °C	-1.6 °C
$MAGST_{max}$	1.0 °C	0.8 °C	2.7 °C	1.0 °C
$MAGST_{avg}$	-0.5 °C	-0.5 °C (0.8 °C)	0.8 °C	0.2 °C (1.3 °C)

5
6
7

1 **Supplementary material**

2 Table S1: Location, vegetation type and period of measurements of ground surface

3 temperature loggers used for the validation.

Latitude	Longitude	Elevation (m)	Vegetation type	Start Year	End Year	No. Years
62.543	6.303	92	Forest	2005	2008	3
62.575	6.317	796	Non-vegetated	2005	2006	1
62.297	9.338	1505	Non-vegetated	2001	2007	6
62.296	9.354	1467	Non-vegetated	2001	2004	3
62.264	9.467	1094	Non-vegetated	2002	2007	5
62.247	9.499	1039	Non-vegetated	2002	2007	5
61.522	12.504	541	Forest	2005	2008	3
61.542	12.439	1022	Non-vegetated	2005	2008	3
60.593	7.526	1210	Non-vegetated	2006	2007	1
60.651	7.493	1559	Non-vegetated	2006	2007	1
60.632	7.496	1431	Non-vegetated	2006	2007	1
60.647	7.489	1508	Non-vegetated	2006	2007	1
60.948	8.152	1220	Non-vegetated	2005	2007	2
62.429	11.274	1538	Non-vegetated	2004	2007	3
62.480	11.293	676	Forest	2006	2008	2
62.447	11.261	1251	Non-vegetated	2006	2008	2
61.721	8.401	1065	Non-vegetated	2004	2007	3
61.707	8.403	1307	Non-vegetated	1999	2007	8
61.702	8.395	1391	Non-vegetated	1999	2002	3
61.702	8.394	1410	Non-vegetated	1999	2002	3
61.701	8.393	1430	Non-vegetated	1999	2002	3
61.701	8.393	1447	Non-vegetated	1999	2008	9
61.699	8.391	1480	Non-vegetated	1999	2001	2
61.699	8.390	1492	Non-vegetated	1999	2000	1
61.685	8.376	1767	Non-vegetated	2004	2007	3
61.678	8.369	1893	Non-vegetated	1999	2004	5
61.677	8.369	1893	Non-vegetated	1999	2007	8
61.678	8.369	1893	Non-vegetated	1999	2004	5
61.649	9.012	855	Forest	2005	2008	3

61.401	8.831	1525	Non-vegetated	2005	2007	2
61.555	8.193	1522	Non-vegetated	2005	2007	2
61.556	8.207	1389	Non-vegetated	2005	2007	2
61.552	8.182	1460	Non-vegetated	2006	2007	1
61.547	8.163	1354	Non-vegetated	2006	2007	1
61.532	8.230	1448	Non-vegetated	2006	2007	1
61.538	8.180	1696	Non-vegetated	2006	2007	1
62.099	8.931	607	Forest	2005	2008	3
62.027	8.925	1573	Non-vegetated	2004	2008	4
59.989	10.670	528	Forest	2003	2006	3
59.980	10.683	443	Forest	2004	2008	4
59.980	10.684	435	Forest	2004	2008	4
60.232	10.428	196	Forest	2006	2008	2
61.934	11.548	805	Non-vegetated	2002	2003	1
61.931	11.543	868	Non-vegetated	2002	2006	4
61.930	11.542	918	Non-vegetated	2002	2006	4
61.927	11.540	1010	Non-vegetated	2002	2006	4
61.925	11.538	1109	Non-vegetated	2002	2006	4
61.922	11.507	987	Non-vegetated	2002	2006	4
61.926	11.511	1051	Non-vegetated	2002	2006	4
61.919	11.536	1211	Non-vegetated	2002	2006	4
61.929	11.527	1043	Non-vegetated	2002	2003	1
61.929	11.527	1043	Non-vegetated	2002	2006	4
61.902	11.500	1069	Non-vegetated	2004	2005	1
61.892	11.504	1078	Non-vegetated	2004	2005	1
61.926	11.535	1071	Non-vegetated	2004	2005	1
61.926	11.535	1071	Non-vegetated	2004	2005	1
61.908	11.537	1418	Non-vegetated	2004	2005	1
61.908	11.537	1418	Non-vegetated	2004	2007	3
61.929	11.527	1043	Non-vegetated	2005	2007	2
62.134	12.020	906	Shrubs	2002	2006	4
62.135	12.055	1196	Non-vegetated	2002	2006	4
62.140	12.060	1316	Non-vegetated	2002	2003	1

62.137	12.053	1207	Non-vegetated	2002	2006	4
62.138	12.051	1192	Non-vegetated	2002	2006	4
62.137	12.030	1052	Non-vegetated	2002	2006	4
62.140	12.060	1316	Non-vegetated	2004	2007	3
62.141	12.061	1335	Non-vegetated	2005	2007	2
69.942	24.862	508	Non-vegetated	2003	2005	2
69.937	24.854	614	Non-vegetated	2003	2005	2
69.913	24.775	1002	Non-vegetated	2003	2005	2
69.910	24.770	1034	Non-vegetated	2003	2005	2
69.909	24.771	982	Non-vegetated	2003	2005	2
69.933	24.789	471	Non-vegetated	2004	2005	1
69.933	24.792	428	Non-vegetated	2004	2005	1
70.075	20.431	839	Non-vegetated	2003	2006	3
70.063	20.451	476	Non-vegetated	2003	2005	2
69.831	21.279	895	Non-vegetated	2002	2008	6
69.838	21.273	700	Non-vegetated	2002	2007	5
69.843	21.259	500	Non-vegetated	2002	2007	5
69.563	20.433	861	Non-vegetated	2002	2007	5
69.576	20.437	685	Non-vegetated	2002	2005	3
69.583	20.435	500	Non-vegetated	2002	2005	3
69.457	20.882	966	Non-vegetated	2006	2007	1
69.354	21.211	786	Non-vegetated	2004	2007	3
69.267	22.481	739	Non-vegetated	2003	2010	7
69.008	23.235	355	Forest	2003	2010	7
69.980	27.269	130	Forest	2003	2009	6
70.542	29.322	502	Non-vegetated	2002	2009	7
70.541	29.342	480	Non-vegetated	2002	2009	7
70.538	29.363	415	Non-vegetated	2002	2009	7
70.537	29.380	355	Non-vegetated	2002	2009	7
70.400	28.200	10	Shrubs	2008	2010	2
70.126	28.593	50	Mire	2008	2010	2
69.376	24.496	284	Non-vegetated	2008	2010	2
69.370	24.082	469	Non-vegetated	2008	2010	2

69.377	24.082	408	Non-vegetated	2008	2010	2
68.996	23.035	308	Shrubs	2008	2010	2
68.755	23.538	380	Shrubs	2008	2010	2
69.580	23.535	380	Shrubs	2008	2010	2
68.749	19.485	1713	Non-vegetated	2008	2010	2
69.292	18.133	1011	Non-vegetated	2007	2011	4
69.638	22.229	923	Non-vegetated	2007	2010	3
61.676	8.365	1861	Non-vegetated	2008	2010	2
61.684	8.372	1771	Non-vegetated	2008	2010	2
61.700	8.385	1559	Non-vegetated	2008	2010	2
61.698	8.401	1561	Non-vegetated	2008	2010	2
61.707	8.403	1314	Non-vegetated	2008	2010	2
61.701	8.393	1450	Non-vegetated	2008	2010	2
62.174	10.702	1630	Non-vegetated	2008	2009	1
62.170	10.703	1589	Non-vegetated	2008	2010	2
62.151	10.715	1290	Shrubs	2008	2010	2
61.903	9.275	1490	Non-vegetated	2008	2010	2
61.898	9.282	1664	Non-vegetated	2008	2010	2
69.291	18.130	990	Non-vegetated	2007	2009	2
69.249	20.445	766	Non-vegetated	2007	2009	2
69.642	22.194	761	Non-vegetated	2007	2010	3
69.681	22.126	570	Non-vegetated	2007	2010	3
62.149	9.378	1047	Non-vegetated	2005	2006	1
69.308	25.341	450	Shrubs	2008	2011	3
69.306	25.340	495	Shrubs	2008	2010	2
69.304	25.338	548	Shrubs	2008	2011	3
69.299	25.330	540	Shrubs	2008	2011	3
69.296	25.326	497	Shrubs	2008	2011	3
69.294	25.318	445	Shrubs	2008	2011	3
69.290	18.131	990	Non-vegetated	2007	2011	4
69.292	18.129	967	Non-vegetated	2007	2011	4
60.700	10.868	264	Forest	1994	2004	10
67.284	14.451	33	Non-vegetated	1994	2004	10

1

1   Table S2: Boreholes used for validation of the permafrost model. x highlights years where

2   data is available.

Borehole	Lat	Lon	Elevation (m)	Depth (m)	08/09	09/10	10/11	11/12	Reference
Abojavri BH1	69.642	22.194	761	6.6	x	X	x		Farbrot et al. 2013
Abojavri BH2	69.681	22.126	570	30.3	x	X			Farbrot et al. 2013
BH31/PACE31	61.676	8.368	1894	20	x	X	x	x	Isaksen et al. 2011
Guolosjavri BH1	69.354	21.211	786	32.3		X	x	x	Farbrot et al. 2013
Guolosjavri BH2	69.366	21.168	814	10.5	x				Farbrot et al. 2013
Guolosjavri BH3	69.356	21.061	780	10.5	x				Farbrot et al. 2013
Iskoras BH2	69.300	25.346	600	58.5		X	x	x	Farbrot et al. 2013
Jetta BH1	61.901	9.285	1560	19.5		X	x		Farbrot et al. 2011
Jetta BH2	61.902	9.234	1450	10		X	x		Farbrot et al. 2011
Jetta BH3	61.905	9.186	1218	10		X	x	x	Farbrot et al. 2011
Juvvass BH1	61.676	8.365	1861	10		X	x	x	Farbrot et al. 2011
Juvvass BH2	61.684	8.372	1771	10		X	x		Farbrot et al. 2011
Juvvass BH3	61.697	8.386	1561	10		X	x		Farbrot et al. 2011
Juvvass BH4	61.700	8.385	1559	10		X	x	x	Farbrot et al. 2011
Juvvass BH5	61.701	8.392	1468	10		X	x	x	Farbrot et al. 2011
Juvvass BH5	61.707	8.403	1314	10		X	x	x	Farbrot et al. 2011
Kistefjellet	69.291	18.130	990	24.8	x				Farbrot et al. 2013
Lavkavagge BH1	69.249	20.445	766	14	x	X	x	x	Farbrot et al. 2013
Lavkavagge BH2	69.239	20.493	600	30.5	x				Farbrot et al. 2013
Lavkavagge BH3	69.224	20.580	492	15.8	x				Farbrot et al. 2013
Tron BH1	62.174	10.702	1640	30		X	x	x	Farbrot et al. 2011
Tron BH2	62.170	10.703	1589	10		X	x	x	Farbrot et al. 2011
Tron BH3	62.151	10.715	1290	10		X	x	x	Farbrot et al. 2011

3